LETTER

doi:10.1038/nature17663

Age and context of the oldest known hominin fossils from Flores

Adam Brumm[1,2]*, Gerrit D. van den Bergh[3]*, Michael Storey[4], Iwan Kurniawan[5]*, Brent V. Alloway[3,6], Ruly Setiawan[3,7], Erick Setiyabudi[5], Rainer Grün[1,8], Mark W. Moore[9], Dida Yurnaldi[3,7], Mika R. Puspaningrum[3], Unggul P. Wibowo[3,5], Halmi Insani[5], Indra Sutisna[5], John A. Westgate[10], Nick J. G. Pearce[11], Mathieu Duval[12], Hanneke J. M. Meijer[13], Fachroel Aziz[5], Thomas Sutikna[3,14], Sander van der Kaars[15,16], Stephanie Flude[17] & Michael J. Morwood[3]‡

Recent excavations at the early Middle Pleistocene site of Mata Menge in the So'a Basin of central Flores, Indonesia, have yielded hominin fossils[1] attributed to a population ancestral to Late Pleistocene *Homo floresiensis*[2]. Here we describe the age and context of the Mata Menge hominin specimens and associated archaeological findings. The fluvial sandstone layer from which the *in situ* fossils were excavated in 2014 was deposited in a small valley stream around 700 thousand years ago, as indicated by $^{40}Ar/^{39}Ar$ and fission track dates on stratigraphically bracketing volcanic ash and pyroclastic density current deposits, in combination with coupled uranium-series and electron spin resonance dating of fossil teeth. Palaeoenvironmental data indicate a relatively dry climate in the So'a Basin during the early Middle Pleistocene, while various lines of evidence suggest the hominins inhabited a savannah-like open grassland habitat with a wetland component. The hominin fossils occur alongside the remains of an insular fauna and a simple stone technology that is markedly similar to that associated with Late Pleistocene *H. floresiensis*.

Mata Menge is located near the northwestern margin of the So'a Basin, a ~400 km^2 geological depression in central Flores (Fig. 1). The basement substrate consists of the Ola Kile Formation (OKF), a greater than 100-m-thick sequence of indurated volcaniclastic deposits[3,4]. Zircon fission-track (ZFT) age determinations date the upper OKF to 1.86 ± 0.12 million years ago (Ma) (ref. 4). The ~5° southward dipping volcanic breccias of the OKF are associated with a former volcanic centre, the Welas Caldera, on the northwestern margin of the basin (Fig. 1). The OKF is unconformably overlaid by the Ola Bula Formation (OBF)[3,4]. A focus of palaeoanthropological research since the 1950s[5–14], the OBF is up to 120 m thick and comprises an intra-basinal fossil- and stone artefact-bearing sequence composed largely of undistorted volcanic, fluvial, and lacustrine sediments deposited between 1.8 and 0.5 Ma[3,4] (Supplementary Information Table 1). An extensive lacustrine sequence—the 'Gero Limestone Member' (GLM)—caps the basin infill and registers the formation of a basin-wide freshwater lake.

The total preserved thickness of the OBF at Mata Menge is 40 m (Fig. 1). The uppermost interval of the GLM, with a thickness of 9 m, crops out on a hill 600 m west (excavation number 35, or E-35). The two main fossil-bearing intervals at Mata Menge form part of a roughly NNW-SSE trending palaeovalley-fill sequence dominantly occupied by cut-and-fill fluviatile and clay-rich, water-supported mass flow deposits (mudflows). The studied upper fossiliferous interval, which contains the hominin fossils, is exposed at the head of a modern stream valley at the base of a hill (height = 397 m). This less than 30-cm-thick OBF sandstone, named Layer II, is well-consolidated, fine- to medium-grained, and contains locally faint parallel laminations in the lower part, as well as numerous water-worn volcanic pebbles (<60 mm). Layer II is discontinuous towards the west and east, and it has an irregular lower bedding plane that cuts down into the underlying unit, a well-developed, consolidated palaeosol (Layer III). A ~6.5-m-thick sequence of mudflow deposits (Layers I-a to I-f) overlies Layer II and is separated from it by a generally sharp contact surface. Layer II represents the deposit of a small, sinuous stream tributary with a NNW to SSE flow direction, as deduced from the slight decrease in elevation of the top of Layer II in the same direction (20 cm over a horizontal distance of 17 m).

We conducted a 50 m^2 excavation (E-32) into Layer II in 2013 (Fig. 1, Extended Data Figs 1 and 2), yielding fossils of *Stegodon florensis*[9], giant rat (*Hooijeromys nusatenggara*, first described in ref. 15), Komodo dragon (*Varanus komodoensis*), and crocodile, as well as stone artefacts (Fig. 2). In 2014, we exposed Layer II over a larger area, recovering seven hominin fossils (six teeth and a mandible fragment), and an undiagnostic hominin cranial fragment[1]. The hominin fossils were embedded in the sandstone matrix of Layer II near the stratigraphic interface with the overlying mudflow deposit (Extended Data Fig. 2).

Layers I-a to I-f are clearly related to eruptive activity within the Welas Caldera, then occupied by a lake. Four articulated thoracic vertebrae of *S. florensis* were recovered from Layer II (Fig. 2k). These are the only articulated stegodont elements so far recovered at Mata Menge, indicating relatively limited post-mortem modification before burial by mudflows. We hypothesize that the artefacts and faunal remains, including hominin elements, were transported short distances by the stream that deposited Layer II, before mudflows originating from within the Welas Caldera inundated these valleys with metre-thick muddy debris. The presence of elements from multiple hominin individuals could be the result of the same volcanic event that triggered the mudflows. Presently, however, it is not possible to estimate the time interval separating the deaths of the hominins from the deposition of the mudflows.

[1]Research Centre of Human Evolution, Environmental Futures Research Institute, Griffith University, Nathan, Queensland 4111, Australia. [2]School of Earth & Environmental Sciences, University of Wollongong, Wollongong, New South Wales 2522, Australia. [3]Centre for Archaeological Science, School of Earth & Environmental Sciences, University of Wollongong, Wollongong, New South Wales 2522, Australia. [4]Quadlab, Natural History Museum of Denmark, University of Copenhagen, DK-1350 Copenhagen, Denmark. [5]Geology Museum, Bandung 40122, Indonesia. [6]School of Geography, Environment and Earth Sciences, Victoria University, Wellington 6012, New Zealand. [7]Center for Geological Survey, Geological Agency, Bandung 40122, Indonesia. [8]Research School of Earth Sciences, The Australian National University, Canberra, Australian Capital Territory 2601, Australia. [9]Stone Tools and Cognition Hub, Archaeology, University of New England, Armidale, New South Wales 2351, Australia. [10]Department of Earth Sciences, University of Toronto, Toronto, Ontario M5S 3B1, Canada. [11]Department of Geography & Earth Sciences, Aberystwyth University, Aberystwyth SY23 3DB, UK. [12]Geochronology, Centro Nacional de Investigación sobre la Evolución Humana (CENIEH), Paseo de Atapuerca, 3, 09002-Burgos, Spain. [13]University Museum of Bergen, University of Bergen, 5007 Bergen, Norway. [14]Pusat Penelitian Arkeologi Nasional (ARKENAS), Jakarta 12510, Indonesia. [15]Cluster Earth & Climate, Faculty of Earth and Life Sciences, Vrije Universiteit, 1081 HV Amsterdam, The Netherlands. [16]School of Earth, Atmosphere and Environment, Monash University, Clayton, Victoria 3800, Australia. [17]School of Geosciences, The University of Edinburgh, Edinburgh EH8 9AD, UK.

*These authors contributed equally to this work.

‡Deceased.

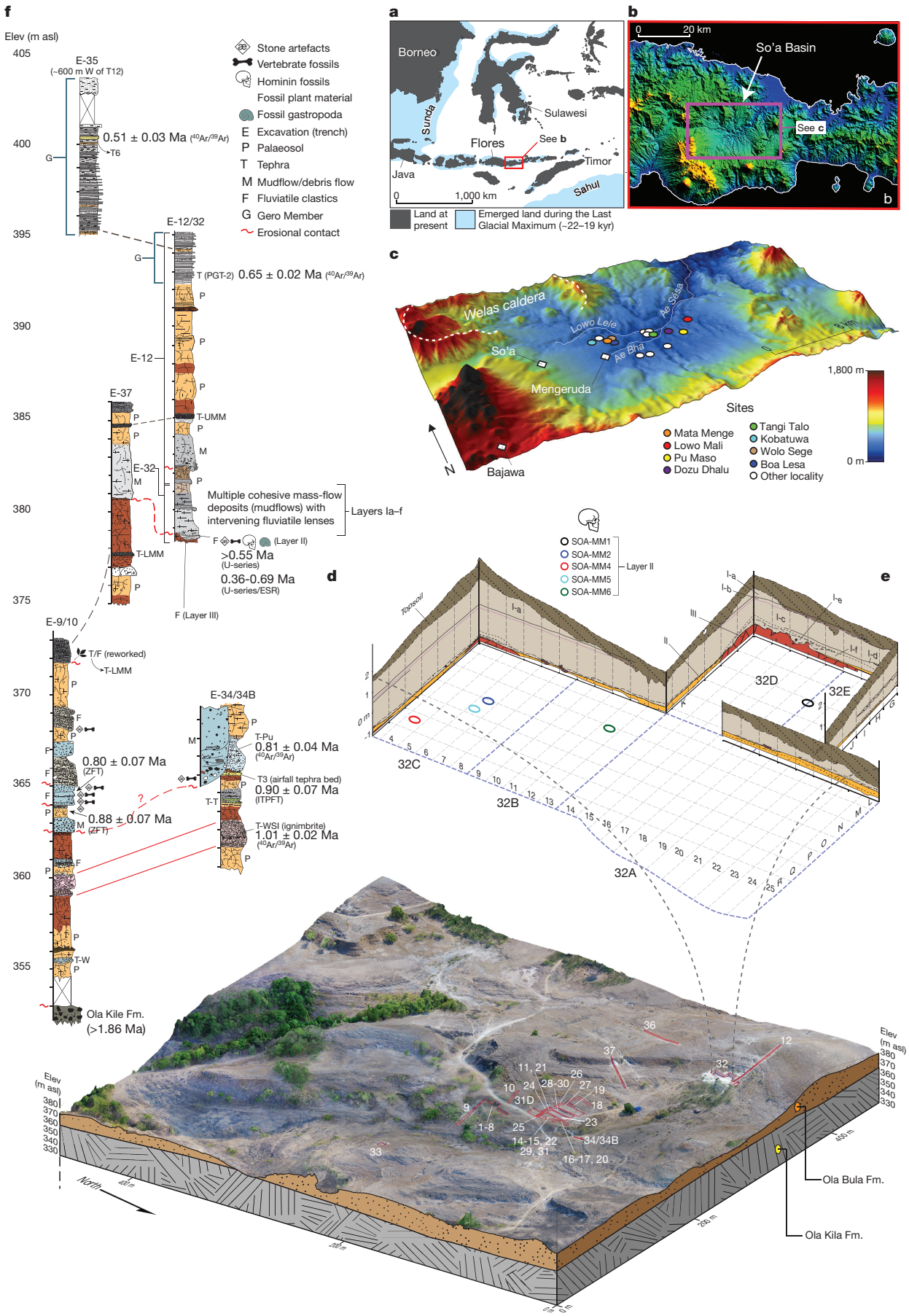

Figure 1 | See next page for caption.

Figure 1 | Context and chronology of the hominin fossils at Mata Menge. a, **b**, location of Flores and the So'a Basin. **c**, Digital elevation map of the So'a Basin, with location of Mata Menge and other sites mentioned in the text. A single outlet of the main river system (the Ae Sésa) drains the basin via a steep-walled valley towards the northeast. **d**, Stratigraphy and chronology of the main fossil-bearing intervals and intervening Ola Bula Formation (OBF) deposits at Mata Menge. Several basin-wide key marker tephra beds that are exposed in the hill flank on the northern side of Mata Menge (trench E-34/34B) are eroded in the central part of the stream valley, where they are replaced by a 4–5-m-thick sequence of tuffaceous mudflows with intervening fluvial lenses forming the lower fossil-bearing palaeovalley-fill sequence. **e**, **f**, Context of the hominin fossils; **f** is a 3D image of Mata Menge and surrounds, with excavated trenches outlined in red and labelled, and **e** is a 3D representation of the stratigraphy exposed by trench E-32A to E, with coloured ovals denoting the positions of *in situ* hominin fossils (SOA-MM1, 2 and 4-6) excavated from the fluvial sandstone unit, Layer II. The remaining hominin specimens were retrieved in the sieves. Trenches E-1 to E-8 were excavated between 2004 and 2006, at the section originally excavated by Th. Verhoeven in the 1950s[5,6]. The remaining trenches were excavated between 2010 and 2015. E-12 is a slot-trench excavated into the side of a hill, revealing an 18-m-thick sequence of lacustrine clays and micritic limestones, fluvial sandstone beds, massive tuffaceous mudflows, well-developed clay-textured palaeosols, and numerous centimetre-thick basaltic tephra inter-beds from the middle-upper part of the OBF. At the base of this slot-trench, a less than 30-cm-thick fossil-bearing sandstone unit (Layer II)—from which all the hominin fossils were retrieved—was exposed. Tephra codes in **d** are as follows (top to bottom): T6 (upper inter-regional tephra); PGT-2 (Piga Tephra 2); T-UMM (Upper Mata Menge Tephra); T-LMM (Lower Mata Menge Tephra); T-Pu (Pu Maso Tephra); T3 (lower inter-regional tephra); T-T (Turakeo Tephra); T-WSI (Wolo Sege Ignimbrite); and T-W (Wolowawu Tephra). The original published $^{40}Ar/^{39}Ar$ age for T-WSI is 1.02 ± 0.02 Ma (ref. 14); however, when recalculated to the recently determined value for the age standard ACS-2 used in this study (1.185 Ma; see reference 25 in the Supplementary Information), T-WSI becomes 1.01 ± 0.02 Ma.

A total of four new radioisotopic age determinations, with ages in sequential order and in accordance with the stratigraphic sequence, provide a chronology for the hominin fossils (Fig. 1; Supplementary Information). Near the base of the OBF at Mata Menge, a widespread ignimbritic marker bed (the Wolo Sege Ignimbrite; T-WSI) with an $^{40}Ar/^{39}Ar$ age of 1.01 ± 0.02 Ma (ref. 14; Fig. 1) is recognized on the combined basis of its stratigraphic association, unique depositional architecture, and glass-shard major element chemistry (Extended Data Fig. 3). In addition, the hominin find-locality in E-32 is situated 12.5 m stratigraphically above a previously reported ZFT date of 0.80 ± 0.07 Ma from Mata Menge[4]. To verify this prior estimate, we conducted isothermal plateau fission-track (ITPFT) dating of glass shards from an inter-regional tephra marker (T3) identified at several So'a Basin localities, including just above the T-WSI at Mata Menge (in E-34/34B), returning a weighted mean age of 0.90 ± 0.07 Ma (based on two independent age determinations) (Supplementary Information Table 2). $^{40}Ar/^{39}Ar$ single crystal dating of hornblende from the Pu Maso Ignimbrite (T-Pu) located just above T3 in E-34/34B yielded a weighted mean age of 0.81 ± 0.04 Ma (Extended Data Fig. 4), which is stratigraphically consistent with that of underlying T3. These ages demonstrate that Layer II was deposited after ~0.80 Ma.

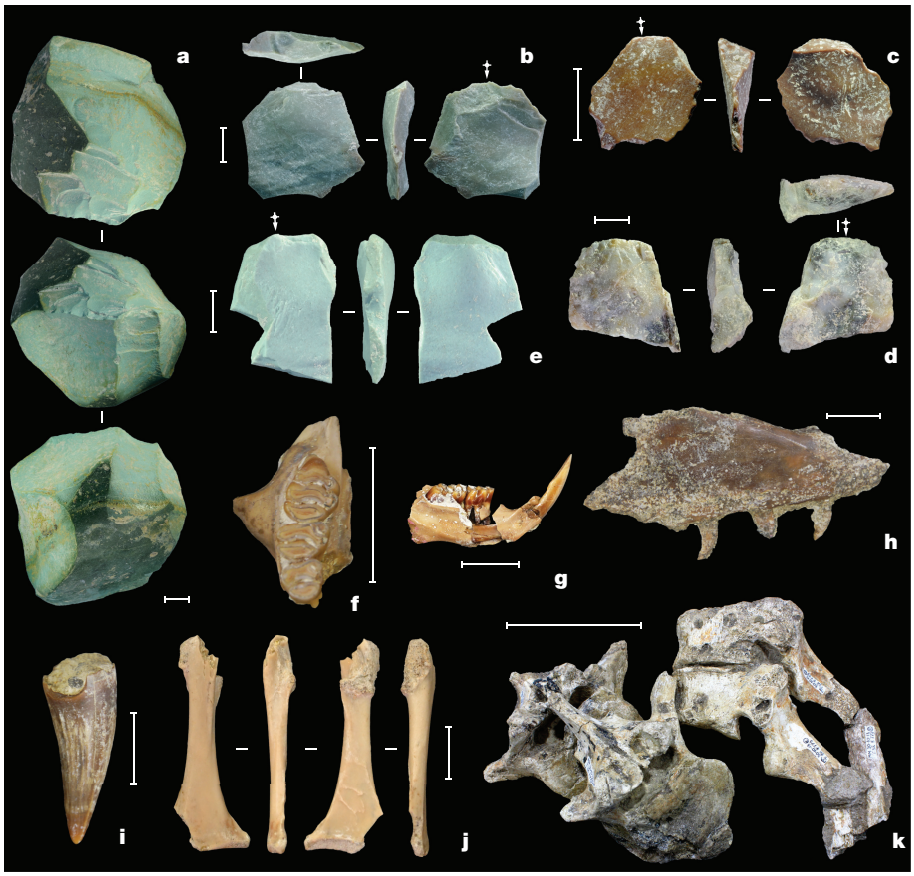

Figure 2 | Stone artefacts and fossils from Mata Menge. All specimens are from the hominin fossil find-locality (Layer II fluviatile sandstone, trench E-32). **a**, Bifacial core (chlorite). **b**, **c**, Chert flakes. **d**, Chalcedony flake. **e**, Rhyolite flake. **f**, Right maxilla fragment (M1-M3), *Hooijeromys nusatenggara*. **g**, Left mandible fragment (m1-m3, i) *H. nusatenggara*. **h**, Right maxilla fragment, *Varanus komodoensis*. **i**, Crocodile tooth. **j**, Right coracoid of a duck (cf. *Tadorna*). **k**, *Stegodon florensis* thoracic vertebrae in articulation (still partially embedded in sandstone matrix). Scale bars, 10 mm (**a**–**j**); 100 mm (**k**).

To further constrain the age of the hominin fossils, we carried out $^{40}Ar/^{39}Ar$ dating on one basaltic tephra and one rhyolitic tephra from the GLM above Layer II (E-12 and E-35). The GLM contains at least 85 crystal-rich tephra inter-beds of basaltic composition, collectively named the Piga Tephra (the lower 56 tephras are sequentially numbered PGT-1 to PGT-56). At Mata Menge, PGT-2 occurs 13.5 m above Layer II, and produced a $^{40}Ar/^{39}Ar$ weighted mean age of 0.65 ± 0.02 Ma from single crystal dating of hornblende (Extended Data Fig. 5). This is in accordance with the published ZFT age of a basaltic tephra inter-bed from the lower part of the GLM (0.65 ± 0.06 Ma)[4]. Finally, a biotite-bearing vitric-rich ash of distinctive rhyolitic composition (T6; Extended Data Fig. 3) from the top of the GLM has an $^{40}Ar/^{39}Ar$ age of 0.51 ± 0.03 Ma, based on the weighted mean of single grain feldspar analyses (Extended Data Fig. 6). Thus, the hominin fossils constrained by the lowermost of these two radioisotopic dates within the GLM have a minimum age of ~0.65 Ma.

We also conducted uranium series (U-series) dating of a hominin tooth root fragment (SOA-MM6) from Layer II, and combined U-series and electron spin resonance (ESR) dating of two *S. florensis* molars excavated *in situ* from the same sedimentary context (Extended Data Fig. 7; Supplementary Information). U-series dating of the hominin tooth root independently confirms that this specimen has an age of at least 0.55 Ma, whereas combined U-series/ESR dating indicates minimum and maximum ages of around 0.36 Ma and 0.69 Ma, respectively, for the *Stegodon* molars. In sum, therefore, we have used multiple dating methods to establish an age of ~0.70 Ma for the hominin fossils.

Our systematic, high volume excavations (~560 m^2) at Mata Menge between 2010 and 2015 yielded many fossil vertebrate remains (Supplementary Information). To date, 75% of the >7,000 vertebrate fossils recovered from E-32 have been analysed, and include *S. florensis* (23.7% of the number of identified specimens (NISP)), *V. komodoensis* (0.6% of NISP), freshwater crocodiles (3.7% of NISP), frogs (0.3% of NISP), murine rodents (15.6% of NISP), and birds (0.5% of NISP), the remainder comprising unidentifiable bone fragments. From the lower fossil-bearing interval (E-1 to 8 and E-11 to 31D), the remains of least 120 *S. florensis* individuals are represented by dental elements spanning all ontogenetic stages[16]. The age profile of this death-assemblage corresponds to that of a living population. The lack of age-selective mortality fits a mass-death event, unlike the juvenile-dominated pattern encountered in the *Stegodon* death-assemblage of the *H. floresiensis* type-locality, Liang Bua[17]. In Layer II, remains of juvenile, sub-adult, intermediate-aged, and old *Stegodon* individuals are also present, but the minimum number of individuals (MNI = 15) is too low to allow construction of a reliable age profile.

We conducted carbon and oxygen isotope analysis of tooth enamel samples collected from several *S. florensis* and murine rodent individuals from the two fossil-bearing levels at Mata Menge (Extended Data Fig. 8). The results indicate a diet dominated by C_4 grasses, suggesting both animals were grazers, and implying that open grasslands were the major vegetation type in the So'a Basin. The recovery of rare fossils of rails, swans, ducks, eagles, and eagle owls from the lower trenches (~0.80 to 0.88 Ma) provides further evidence for the presence of a savannah-like biome with wetland habitats, as well as scattered patches of forest[18]. Fossil pollen and phytoliths from both fossil levels offer additional indications that grasses dominated the early Middle Pleistocene vegetation (Supplementary Information Table 9). Abundant moulds and casts of two freshwater gastropod species (*Cerithidea*) were recovered from Layer II, pointing to the existence of permanent freshwater bodies in the ancestral stream valley.

Our excavations uncovered 149 *in situ* stone artefacts in E-32, including 47 artefacts from Layer II, in direct association with the hominin remains (Fig. 2; Extended Data Fig. 9). Some of the artefacts from E-32 are lightly to heavily abraded from low-energy water transport[19], but 74.5% are in fresh, as-struck condition, suggesting minimal dislocation from nearby stone-flaking areas. Overall, the E-32 assemblage reflects a technologically straightforward core-and-flake approach to stoneworking[20]. As yet, no butchery marks have been identified on the faunal remains at Mata Menge.

Notably, the tools and flaking technology in E-32 are nearly identical in size and nature, respectively, to the assemblage dating some 110 thousand years (kyr) earlier at Mata Menge[13,21–23], including 1,186 analysed stone artefacts from E-23 and E-27 excavated between 2011 and 2014 (Supplementary Information Table 6). The E-32 assemblage is also technologically similar to the artefacts from Liang Bua, dating ~600 kyr later[13,24] and associated with *H. floresiensis*[25,26]. The long persistence of this technology[13] suggests stability in the behaviour of *H. floresiensis*[1]. In contrast, the only lithic assemblage recovered *in situ* below the T-WSI—which has a minimum age of 1.01 ± 0.02 Ma and is the oldest known technology from Flores[14]—while similar, features a typologically distinct element: large Acheulean pick-like implements[27] associated elsewhere with cognitively advanced tool-making[20,28–30]. It is unclear why these artefacts are absent from the later technology of Flores. A shift to more arid conditions could have stimulated a series of technological changes. Alternatively, the earliest inhabitants of Flores may have responded to the limited resources of the island by reducing the complexity of their tool-making repertoire to the minimum required for survival.

Online Content Methods, along with any additional Extended Data display items and Source Data, are available in the online version of the paper; references unique to these sections appear only in the online paper.

Received 30 December 2015; accepted 11 March 2016.

1. van den Bergh, G. D. *et al. Homo floresiensis*-like hominin fossils from the early Middle Pleistocene of Flores. *Nature* http://dx.doi.org/10.1038/nature17999 (2016).
2. Brown, P. *et al.* A new small-bodied hominin from the Late Pleistocene of Flores, Indonesia. *Nature* **431,** 1055–1061 (2004).
3. Morwood, M. J., O'Sullivan, P. B., Aziz, F. & Raza, A. Fission-track ages of stone tools and fossils on the east Indonesian island of Flores. *Nature* **392,** 173–176 (1998).
4. O'Sullivan, P. B. *et al.* Archaeological implications of the geology and chronology of the Soa Basin, Flores, Indonesia. *Geology* **29,** 607–610 (2001).
5. Maringer, J. & Verhoeven, Th. Die Steinartefakte aus der *Stegodon*-Fossilschicht von Mengeruda auf Flores, Indonesien. *Anthropos* **65,** 229–247 (1970).
6. Maringer, J. & Verhoeven, Th. Die Oberflächenfunde aus dem Fossilgebiet von Mengeruda und Olabula auf Flores, Indonesien. *Anthropos* **65,** 530–546 (1970).
7. Sondaar, P. Y. *et al.* Middle Pleistocene faunal turn-over and colonisation of Flores (Indonesia) by *Homo erectus*. *C. R. Acad. Sci.* **319,** 1255–1262 (1994).
8. Morwood, M. J. *et al.* Stone artefacts from the 1994 excavation at Mata Menge, West Central Flores, Indonesia. *Aust. Archaeol*. **44,** 26–34 (1997).
9. van den Bergh, G. D. *The Late Neogene Elephantoid-Bearing Faunas of Indonesia and their Palaeozoogeographic Implications. A Study of the Terrestrial Faunal Succession of Sulawesi, Flores and Java, including Evidence for Early Hominid Dispersal East of Wallace's Line* (Scripta Geologica 117, Nationaal Natuurhistorisch Museum, 1997).
10. van den Bergh, G. D. *et al.* Did *Homo erectus* reach the island of Flores? *Bull. Indo. Pac. Pre. Hi.* **14,** 27–36 (1996).
11. Morwood, M. J. *et al.* Archaeological and palaeontological research in central Flores, east Indonesia: results of fieldwork 1997–98. *Antiquity* **73,** 273–286 (1999).
12. Aziz, F. & Morwood, M. J. in *Pleistocene Geology, Palaeontology and Archaeology of the Soa Basin, Central Flores, Indonesia* (eds Aziz, F., Morwood, M. J. & van den Bergh, G. D.) 1–18 (Spec. Publ. 36, Geological Survey Institute, 2009).
13. Brumm, A. *et al.* Early stone technology on Flores and its implications for *Homo floresiensis*. *Nature* **441,** 624–628 (2006).
14. Brumm, A. *et al.* Hominins on Flores, Indonesia, by one million years ago. *Nature* **464,** 748–752 (2010).
15. Musser, G. G. The giant rat of Flores and its relatives east of Borneo and Bali. *Bull. Am. Mus. Nat. Hist.* **169,** 67–176 (1981).
16. van den Bergh, G. D. *et al.* Taphonomy of *Stegodon florensis* remains from the early Middle Pleistocene archaeological site Mata Menge, Flores, Indonesia. Abstract book of the VIth International Conference on Mammoths and their relatives. *S.A.S.G.*, Special Volume **102,** 207–208 (2014).
17. van den Bergh, G. D. *et al.* The youngest *Stegodon* remains in Southeast Asia from the Late Pleistocene archaeological site Liang Bua, Flores, Indonesia. *Quat. Int.* **182,** 16–48 (2008).
18. Meijer, H. J. M. *et al.* Avian remains from the Early/Middle Pleistocene of the So'a Basin, central Flores, Indonesia, and their palaeoenvironmental significance. *Palaeogeogr. Palaeocl*. **440,** 161–171 (2015).

19. Shea, J. J. Artifact abrasion, fluvial processes, and ''living floors'' from the Early Paleolithic site of 'Ubeidiya (Jordan Valley, Israel). *Geoarchaeology* **14,** 191–207 (1999).
20. Moore, M. W. The design space of stone flaking: implications for cognitive evolution. *World Archaeol.* **43,** 702–715 (2011).
21. Brumm, A. *et al.* Stone technology at the Middle Pleistocene site of Mata Menge, Flores, Indonesia. *J. Arch. Sci.* **37,** 451–473 (2010).
22. Moore, M. W. & Brumm, A. Stone artifacts and hominins in island Southeast Asia: new insights from Flores, eastern Indonesia. *J. Hum. Evol.* **52,** 85–102 (2007).
23. Moore, M. W. & Brumm, A. *Homo floresiensis* and the African Oldowan in *Interdisciplinary Approaches to the Oldowan* (eds Hovers, E. & Braun, D. R.) 61–69 (Springer, 2009).
24. Moore, M. W. *et al.* Continuities in stone flaking technology at Liang Bua, Flores, Indonesia. *J. Hum. Evol.* **57,** 503–526 (2009).
25. Morwood, M. J. *et al.* Archaeology and age of a new hominin from Flores in eastern Indonesia. *Nature* **431,** 1087–1091 (2004).
26. Sutikna, T. *et al.* Revised stratigraphy and chronology for *Homo floresiensis* at Liang Bua in Indonesia. *Nature* **532,** 366–369 (2016).
27. Brumm, A. & Moore, M. W. Biface distributions and the Movius Line: a Southeast Asian perspective. *Aust. Archaeol.* **74,** 32–46 (2012).
28. Beyene, Y. *et al.* The characteristics and chronology of the earliest Acheulean at Konso, Ethiopia. *Proc. Natl Acad. Sci. USA* **110,** 1584–1591 (2013).
29. Wynn, T. Archaeology and cognitive evolution. *Behav. Brain Sci.* **25,** 389–402 (2002).
30. Gowlett, J. A. J. The elements of design form in Acheulian bifaces: modes, modalities, rules and language, in *Axe Age: Acheulian Tool-making From Quarry to Discard* (eds Goren-Inbar, N. & Sharon, G.) 203–221 (Equinox, 2006).

Supplementary Information is available in the online version of the paper.

Acknowledgements The So'a Basin project was funded by an Australian Research Council (ARC) *Discovery* grant (DP1093342) awarded to M.J.M. and A.B., and directed by M.J.M. (2010–2013) and G.v.d.B. (2013–2015). The Geological Survey Institute (GSI) of Bandung, Indonesia, provided additional financial and technical support. G.v.d.B.'s research was also supported by ARC Future Fellowship FT100100384. M.W.M. was funded by ARC grant DP1096558. Quadlab is funded by a grant to M.S. from the Villum Foundation. M.D. received funding from a Marie Curie International Outgoing Fellowship of the EU's Seventh Framework Programme (FP7/2007-2013), awarded under REA Grant Agreement No. PIOF-GA-2013-626474. B.V.A. received funding from a Victoria University of Wellington Science Faculty Research Grant (201255). For permission to undertake this research, we thank the Indonesian State Ministry of Research and Technology (RISTEK), the former Heads of the Geological Agency (R. Sukyiar and Surono), the successive directors of the GSI (S. Permanandewi, Y. Kusumahbrata (formerly) and A. Pribadi) and Bandung's Geology Museum (S. Baskoro and O. Abdurahman). Local research permissions were issued by the provincial government of East Nusa Tenggara at Kupang, and the Ngada and Nage Keo administrations. We also thank the Ngada Tourism and Culture and Education Departments for their ongoing support. In addition, we acknowledge support and advice provided by I. Setiadi, D. Pribadi, and Suyono (GSI), the Pusat Penelitian Arkeologi Nasional (ARKENAS) in Jakarta, and J. T. Solo of the provincial Culture and Tourism office in Kupang. Scientific and technical personnel involved in the fieldwork included: T. Suryana, S. Sonjaya, H. Oktariana, I. Sutisna, A. Rahman, S. Bronto, E. Sukandar, A. Gunawan, Widji, A. T. Hascaryo, Jatmiko, S. Wasisto, R. A. Due, S. Hayes, Y. Perston, B. Pillans, K. Grant, M. Marsh, D. McGahan, A. M. Saiful, B. Burhan, L. Siagian, D. Susanti, P. D. Moi, M. Tocheri, A. R. Chivas, and A. Cahyana. F. Wesselingh identified gastropod remains. Sidarto (GSI) provided digital elevation model data used in Fig. 1b. Geodetic surveys and measurements were conducted by E. E. Laksmana, A. Rahmadi, Y. Sofyan, and G. Hazell. J. Noblett constructed the Mata Menge 3D model, based on drone aerial photographs taken by K. Riza, T. P. Ertanto, and M. Faizal. The research team was supported by ~100 excavators and support personnel from the Ngada and Nage Keo districts. We thank L. Kinsley, Research School of Earth Sciences, The Australian National University, for assistance with mass spectrometric measurements.

Author Contributions A.B., G.D.v.d.B., I.K. and M.J.M. directed the Mata Menge excavations. M.S., B.V.A. and R.S. collected tephra samples and M.S. undertook $^{40}Ar/^{39}Ar$ dating. G.D.v.d.B. described the site stratigraphy, with R.S., D.Y., S.F. and B.V.A. ITPFT-dating of T3 was jointly conducted by J.A.W. and B.V.A., while EMP analyses of all So'a Basin tephra were conducted by B.V.A. and R.S. Comparative trace element analyses of interregional tephra markers were jointly undertaken by J.A.W., N.J.G.P. and B.V.A. E.S., F.A. and T.S. oversaw key aspects of the field project. M.W.M. analysed the stone assemblage, and G.D.v.d.B., H.I., I.S., M.R.P., U.P.W. and H.J.M.M. analysed the fauna. M.R.P. conducted isotopic analyses, R.G. and M.D. undertook U/Th and ESR analyses of faunal remains, and S.v.d.K. carried out the palynological analysis. A.B. and G.D.v.d.B. prepared the manuscript, with contributions from other authors.

Author Information Reprints and permissions information is available at www.nature.com/reprints. The authors declare no competing financial interests. Readers are welcome to comment on the online version of the paper. Correspondence and requests for materials should be addressed to G.D.v.d.B. (gert@uow.edu.au) or A.B. (a.brumm@griffith.edu.au).

METHODS

For isothermal plateau fission track (ITPFT) dating of hydrated glass shards[31], the population-subtraction technique was applied[32,33]. This technique is grain specific, in that every grain is examined separately under the microscope and a mean age is derived from a large number of shards. In this case, contamination can be readily monitored, and, if necessary, checked by electron microprobe analysis (EMA) of individual shards. Chemical homogeneity indicates derivation from a single eruptive event with a strong likelihood of uniform U content. Chunky, low vesicular glass shards in the size range of 500–250 μm were separated in order to maximise the surface area of the glass in the polished section and to optimise fission-track counting. ITPFT ages for T3 at two So'a Basin localities (Kopowatu, UT2382 and Lowo Mali, UT2383) are given in Supplementary Information Table 2, as well as operating conditions and the ages determined on the Huckleberry Ridge tephra internal standard. The single-crystal (sanidine) laser-fusion $^{40}Ar/^{39}Ar$ age of Huckleberry Ridge tephra is 2.003 ± 0.014 Ma (2σ error)[34], and is indistinguishable from the PTF-corrected age of 2.08 ± 0.21 Ma determined on UT1366 using the diameter-corrected procedure (DCFT)[35] (see Supplementary Information Table 2). All samples were irradiated at the same time in a single can. Ages were calculated using the zeta approach and $\lambda_D = 1.551 \times 10^{-10}$ per year. Zeta value is 301 ± 3 based on 6 irradiations, using the NIST SRM 612 glass dosimeter and the Moldavite tektite glass (Lhenice locality) with an $^{40}Ar/^{39}Ar$ plateau age of 14.34 ± 0.08 Ma (refs 36,37). Ages are those corrected for partial track fading (PTF), achieved by the isothermal plateau method (ITPFT)[31] and the diameter-corrected procedure (DCFT)[35]. Following irradiation, both T3 samples were subjected to a single heat treatment of 150°C for 30 days. After heating, the spontaneous and induced sample slides were simultaneously etched in 24% HF for 110 s. The Ds and Di track diameters were then measured and the Ds/Di ratio determined. Provided that the Ds/Di ratio was close to unity and that the samples were adequately etched — as evidenced by the average track diameters being within the range of 6–8 μm (ref. 31) — the samples were corrected for partial track fading (PTF) and the track densities determined. Area was then estimated using the point-counting method. The corresponding ρs/ρi ratio is equivalent to the true track density ratio. The age calculated from this ratio is therefore equivalent to the true age of the sample. The precision of ITPFT ages for some samples was improved by independent determinations made by different operators, in some cases using slightly different etching conditions. The weighted mean age and error of corrected ages for UT2382 and UT2383 is 0.90 ± 0.07 Ma (see Supplementary Table 2).

Glass shard major element determinations. Glass shard major element determinations were conducted on all rhyolitic pyroclastic density current (PDC) and airfall deposits at Mata Menge, as well as potential correlatives from other So'a Basin sites. Glass shard major element data was acquired with a JEOL Superprobe (JXA-8230), using the ZAF correction method. Analyses were performed with 15 kV accelerating voltage, 8 nA beam current, and an electron beam defocused to between 20 to 10 μm. Standardization was achieved by means of mineral and glass standards. A rhyolitic glass standard (ATHO-G) was routinely used to monitor calibration in all analytical runs, and used to evaluate any day-to-day differences in the calibration. The large number of samples precluded conducting all analyses in a single batch. All analyses are normalized to 100 wt. % anhydrous, with H_2O by difference being given, and total Fe is reported as FeO. Glass shard major element analyses are presented in Supplementary Information Table 3. Trace element analyses were conducted on individual glass shards from two distinct rhyolitic tephra marker beds of presumed distal source (T3 correlatives from Mata Menge, Lowo Mali and Kopowatu, and T6 from Mata Menge, respectively). This trace element data was then directly compared with reference data from potential distal tephra correlatives (that is, Youngest Toba Tuff (YTT), Middle Toba Tuff (MTT), Oldest Toba Tuff (OTT) and Unit E from ODP-758) acquired on the same instrument using the same standards and under the same analytical conditions[38,39] (see Extended Data Fig. 3i–m). Trace element analyses were performed by laser ablation (LA) ICP-MS, using a Coherent GeoLas ArF 193 nm Excimer LA system coupled to a Thermo Finnegan Element 2 sector field ICP-MS. Trace element data were collected for individual shards, with the majority of analyses performed using 20 μm ablation craters. Laser fluence was 10 Jcm^{-2} at a repetition rate of 5 Hz for a 24 s acquisition. The minor ^{29}Si isotope was used as the internal standard, with SiO_2 (determined by EMPA) used to calibrate each analysis, after normalization to an anhydrous basis. The NIST 612 reference glass was used for calibration, taking concentrations from established sources[40]. A fractionation factor was applied to the data to account for analytical bias related to the different matrices of the reference standard and the sample. Explication of this factor as well as ICP-MS and laser operating conditions is given elsewhere[41]. The MPI-DING reference glass ATHO-G (ref. 42) was analysed as an unknown under the same operating conditions at the same time. Analytical precision is typically between ±5–10%, and accuracy is typically around ±5%, when compared with the published GeoReM concentrations for ATHO-G. Glass shard trace element analyses are presented in Supplementary Information Table 4.

Single crystal laser fusion $^{40}Ar/^{39}Ar$ dating. We conducted single crystal laser fusion $^{40}Ar/^{39}Ar$ dating of the Mata Menge volcanic units. Hornblende crystals (<2 mm in length) from the basaltic PGT-2 tephra sample (T XII 252-261) were pre-concentrated along with other ferromagnesian minerals using standard heavy liquid techniques and then distinguished from pyroxene using a Bruker micro-xrf, followed by handpicking of individual grains under a binocular microscope. For the other samples, hornblende (1–2 mm in length from FLO15-15) and small feldspar crystals (<0.5 mm in length from FLO15-09/2) were handpicked under a binocular microscope from the sieved and washed <2 mm size fraction. Crystals were loaded into wells in 18 mm-diameter aluminium sample discs for neutron irradiation, along with the Alder Creek sanidine age standard (ACs-2)[43] as the neutron fluence monitor. In this study, we report our age determinations relative to the recently published and astronomically calibrated 1.185 Ma value for ACs-2 (ref. 44). Neutron irradiation was performed in two batches (QL-OSU-39 and QL-OSU-42), each with a duration of 15 min, in the cadmium-shielded CLICIT facility at the Oregon State University TRIGA reactor. Argon isotopic analyses of gas released during the CO_2 laser single crystal fusion experiments (Supplementary Information Table 5) were made on a fully automated Nu Instruments Noblesse multi-collector noble-gas mass spectrometer, using procedures documented previously[14,45]. Reconnaissance isotopic measurements of small gas aliquots released from feldspar crystals during an initial low-temperature heating step, using a low-power defocused laser beam, allowed the identification of scarce, K-rich grains within a population dominated by Ca-rich, K-poor plagioclase; the latter not being amenable to $^{40}Ar/^{39}Ar$ dating because of small signal size. Fusion experiments on eight of these relatively K-rich grains identified by this prospecting method yielded small but measurable amounts of ^{40}Ar (7.5×10^{-17} to 1.3×10^{-15} mol ^{40}Ar) and ^{39}Ar. Sample gas cleanup was through an all-metal extraction line, equipped with a –130°C cold trap (to remove H_2O) and two water-cooled SAES GP-50 getter pumps (to absorb reactive gases). Argon isotopic analyses of unknowns, blanks, and monitor minerals were carried out in identical fashion during a fixed period of 400 s in 14 data acquisition cycles. ^{40}Ar and ^{39}Ar were measured on the high-mass ion counter, ^{38}Ar and ^{37}Ar on the axial ion counter and ^{36}Ar on the low-mass ion counter, with baselines measured every third cycle. Measurement of the ^{40}Ar, ^{38}Ar, and ^{36}Ar ion beams was carried out simultaneously, followed by sequential measurement of ^{39}Ar and ^{37}Ar. Beam switching was achieved by varying the field of the mass spectrometer magnet and with minor adjustment of the quad lenses. Data acquisition and reduction was performed using the program 'Mass Spec' (A. Deino, Berkeley Geochronology Center). J-values for unknowns were calculated by using a plane-fitting algorithm in the Mass Spec software applied to ACs-2 standard data from symmetrically distributed sample wells across the aluminium irradiation disk (Supplementary Information Table 5). Detector intercalibration and mass fractionation corrections were made using the weighted mean of a time series of measured atmospheric argon aliquots delivered from a calibrated air pipette[14,45]. Sample sets were bracketed by both air pipette and ACs-2 to monitor for possible instrumental drift. Blanks were measured at least once before each run of an unknown and had typical values of $<1.5 \times 10^{-16}$ mol ^{40}Ar and $<1 \times 10^{-18}$ mol ^{36}Ar for QL-OSU-39 experiments, and $2\text{-}3 \times 10^{-16}$ mol ^{40}Ar and $<2.5 \times 10^{-18}$ mol ^{36}Ar for those of QL-OSU-42. The higher blanks of the QL-OSU-42 experiments can be attributed to the venting and baking of the Noblesse mass-spectrometer after the completion of QL-OSU-39 analyses. Decay and other constants, including correction factors for interference isotopes produced by nucleogenic reactions, are given in Supplementary Information Table 5.

Laser ablation U-series analyses. Laser ablation U-series analyses were carried out on two fragments of the same hominin incisor ((SOA-MM6) sample number 3543A: a fragment of the tooth crown, including portions of dentine and enamel tissues; and sample number 3543B, a cross-section of the root of SOA-MM6 only), as well as on two *Stegodon florensis* molars (sample number 3541, and a molar broken into two fragments, which we subdivided respectively into sample number 3542, and sample number 3544). The experimental setup, measurement conditions, and data evaluation followed principles and procedures described in ref. 46. The dentine and enamel tissues of sample number 3543A were analysed on different tracks, whereas three tracks were analysed across the root section (sample number 3543B). The *Stegodon* molars were analysed along several tracks that cut across the dental tissues. No individual age calculation was carried when the U-concentrations were below about 0.5 ppm and detrital ^{232}Th was observed (elemental U/Th ratios below 300). The analytical data of the enamel and dentine sections were integrated to provide the data input for the ESR age calculations. All results are shown in Supplementary Information Table 6. ESR dating was also performed on the two *S. florensis* molars noted above. The fossil teeth were prepared following a standard ESR dating procedure for enamel powder[47]. The grey

enamel layer was mechanically separated from the other dental tissues, and both inner and outer surfaces were removed with a dental drill to eliminate the volume that had received an external alpha dose. The samples were then ground and sieved to recover the size fraction of $<200\,\mu m$. Dose evaluation used the multiple aliquot additive dose method. The powder was split into several aliquots and irradiated up to 4019 Gy with a Gammacell 1000 Cs-137 gamma source. ESR measurements were carried out with a Bruker Elexsys 500 spectrometer, using the following acquisition parameters: 3–5 scans, 2 mW microwave power, 1024 points resolution, 12 mT sweep width, 50 kHz modulation frequency, 0.1 mT modulation amplitude, 20 ms conversion time and 5 ms time constant. The ESR intensities were extracted from T1-B2 peak-to-peak amplitudes of the ESR signal[48], and then normalized on the number of scans and mass. All aliquots of a given sample were measured within a short time interval (<1 h). This procedure was repeated twice over two successive days without removing the enamel from the ESR tubes between measurements in order to evaluate measurement precision and thus D_E reproducibility: the latter was found to be excellent, with a variability of $<3\%$ between the two repeated measurements. Fitting procedures were carried out with the Microcal OriginPro 9.1 software using a Levenberg-Marquardt algorithm by chi-square minimisation. Data were weighted by the inverse of the squared ESR intensity ($1/I^2$) (ref. 49). Final equivalent dose (D_E) values were obtained by fitting a single saturating exponential (SSE) through the pooled ESR intensities obtained from the two repeated measurements. Given the magnitude of the D_E values (between 400 Gy and 600 Gy), a maximum irradiation dose (D_{max}) of 4019 Gy was used, so that D_{max}/D_E ratio remains between 5 and 10 as recommended in a recent study[50] to ensure reliable fitting. The final dose response curves (DRCs) are shown in Extended Data Fig. 7f, g. For the dose rate calculations, the following parameters were used: an alpha efficiency of 0.13 ± 0.02 (ref. 51), Monte-Carlo beta attenuation factors from ref. 52, dose-rate conversion factors from ref. 53, an estimated water content of 5 ± 3 wt.% in dentine and 20 ± 5 wt.% in sediment. U and Th and K concentrations in raw sediment were determined by ICP-OES and ICP-MS analysis on samples collected within Layer II (Supplementary Information Table 7). The mean radioelement concentration values were used for the age calculations. Combined U-series/ESR ages were calculated with DATA, a DOS-based programme[54] using the US model defined in ref. 55, and considering the following geometry: sediment/brown enamel/grey enamel/dentine. Further details about this dating method as applied to fossil teeth may be found elsewhere[56]. The results of the age calculations are shown in Supplementary Information Table 8.

31. Westgate, J. A. Isothermal plateau fission-track ages of hydrated glass shards from silicic tephra beds. *Earth Planet. Sci. Lett.* **95,** 226–234 (1989).
32. Westgate, J. A. Fission track dating of volcanic glass, in *Encyclopedia of Scientific Dating Methods* (eds. Rink, W. J. & Thompson, J.) 1–60 (Springer Dordrecht, 2014).
33. Westgate, J. A., Naeser, N. D. & Alloway, B. V. Fission-track dating, in *The Encyclopedia of Quaternary Science* (ed. Elias, S.) 643–662 (Elsevier, 2013).
34. Gansecki, C. A., Mahood, G. A. & McWilliams, M. New ages for the climactic eruptions of Yellowstone: single-crystal $^{40}Ar/^{39}Ar$ dating identifies contamination. *Geology* **26,** 343–346 (1998).
35. Sandhu, A. S. & Westgate, J. A. The correlation between reduction in fission-track diameter and areal track density in volcanic glass shards and its application in dating tephra beds. *Earth Planet. Sci. Lett.* **131,** 289–299 (1995).
36. Laurenzi, M. A. *et al.* $^{40}Ar/^{39}Ar$ laser probe dating of the Central European tektite-producing impact event. *Meteorit. Planet. Sci.* **38,** 887–893 (2003).
37. Laurenzi, M. A. *et al.* New constraints on ages of glasses proposed as reference materials for fission-track dating. *Geostand. Geoanal. Res.* **31,** 105–124 (2007).
38. Pearce, N. J. G. *et al.* Individual glass shard trace element analyses confirm that all known Toba tephra reported from India is from the c. 75-ka Youngest Toba eruption. *Journ. Quat. Sci.* **29,** 729–734 (2014).
39. Westgate, J. A. & Pearce, N. J. G. Quaternary tephrochronology of the Toba tuffs and its significance with respect to archaeological studies in peninsular India, in *Issues in Indian Archaeology: Prehistory to Early History* (ed. Korisettar, R.) (Primus Books New Delhi, in press).
40. Pearce, N. J. G. *et al.* A compilation of new and published major and trace element data for NIST SRM 610 and NIST SRM 612 glass reference materials. *Geost. Newslet.* **21,** 115–144 (1997).
41. Pearce, N. J. G. *et al.* Trace-element analysis by LA-ICP-MS: the quest for comprehensive chemical characterisation of single sub-10 μm volcanic glass shards. *Quat. Int.* **246,** 57–81 (2011).
42. Jochum, K. P. *et al.* MPI-DING reference glasses for in-situ microanalysis: new reference values for element concentrations and isotope ratios. *Geochem. Geophys. Geosys.* **7,** Q02008 (2006).
43. Nomande, S. *et al.* Alder Creek sandidine (ACs-2): a Quaternary 40Ar/39Ar dating standard tied to the Cobb Mountain geomagnetic event. *Chem. Geol.* **218,** 315–338 (2005).
44. Rivera, T. A., Storey, M., Schmitz, M. D. & Crowley, J. L. Age intercalibration of $^{40}Ar/^{39}Ar$ sanidine and chemically distinct U/Pb zircon populations from the Alder Creek Rhyolite Quaternary geochronology standard. *Chem. Geol.* **345,** 87–98 (2013).
45. Storey, M., Roberts, R. G. & Saidin, M. Astronomically calibrated $^{40}Ar/^{39}Ar$ age for the Toba supereruption and global synchronization of late Quaternary records. *Proc. Natl Acad. Sci. USA* **109,** 18684–18688 (2012).
46. Grün, R. *et al.* Laser ablation U-series analysis of fossil bones and teeth. *Palaeogeogr. Palaeocl.* **416,** 150–167 (2014).
47. Duval, M. *et al.* The challenge of dating Early Pleistocene fossil teeth by the combined uranium series–electron spin resonance method: the Venta Micena palaeontological site (Orce, Spain). *J. Quaternary Sci.* **26,** 603–615 (2011).
48. Grün, R. Methods of dose determination using ESR spectra of tooth enamel. *Radiat. Meas.* **32,** 767–772 (2000).
49. Grün, R. & Brumby, S. The assessment of errors in past radiation doses extrapolated from ESR/TL dose-response data. *Radiat. Meas.* **23,** 307–315 (1994).
50. Duval, M. & Grün, R. Are published ESR dose assessments on fossil tooth enamel reliable? *Quat. Geochronol.* **31,** 19–27 (2016).
51. Grün, R. & Katzenberger-Apel, O. An alpha irradiator for ESR dating. *Ancient TL* **12,** 35–38 (1994).
52. Marsh, R. E. *Beta-gradient Isochrons Using Electron Paramagnetic Resonance: Towards a New Dating Method in Archaeology*. MSc thesis, McMaster University (1999).
53. Adamiec, G. & Aitken, M. J. Dose-rate conversion factors: update. *Ancient TL* **16,** 37–50 (1998).
54. Grün, R. The DATA program for the calculation of ESR age estimates on tooth enamel. *Quat. Geochronol.* **4,** 231–232 (2009).
55. Grün, R., Schwarcz, H. P. & Chadam, J. M. ESR dating of tooth enamel: coupled correction for U-uptake and U-series disequilibrium. *Nucl. Tracks Radiat. Meas.* **14,** 237–241 (1988).
56. Duval, M. Electron Spin Resonance (ESR) dating of fossil tooth enamel, in *Encyclopedia of Scientific Dating Methods* (eds. Rink, W. J. & Thompson, J.) 1–11 (Springer Dordrecht, 2015).
57. Deino, A. & Potts, R. Age-probability spectra for examination of single-crystal $^{40}Ar/^{39}Ar$ dating results: examples from Olorgesailie, southern Kenya Rift. *Quat. Int.* **13–14,** 47–53 (1992).
58. Powell, R., Hergt, J. & Woodhead, J. Improving isochron calculations with robust statistics and the bootstrap. *Chem. Geol.* **185,** 191–204 (2002).
59. Lee, J.-Y. *et al.* A redetermination of the isotopic abundances of atmospheric Ar. *Geochim. Cosmochim. Acta* **70,** 4507–4512 (2006).
60. Moore, M. W. *et al.* Continuities in stone flaking technology at Liang Bua, Flores, Indonesia. *J. Hum. Evol.* **57,** 503–526 (2009).

Extended Data Figure 1 | Hominin fossil find-locality at Mata Menge. **a**, View of Excavation 32 (trench E-32) in 2014, taken towards the north-north-west. The dip slope visible in the background is the eastern flank of the Welas Caldera, which was the source for many of the volcanic products deposited in the So'a Basin. **b**, trench E-32A to E viewed towards the southwest, in October 2015. **c**, E-32D to E-32E viewed towards the southwest. The irregular erosional upper surface of the reddish brown palaeosol (Layer III) formed the hardened bedding of a small stream. The sandy fossil-bearing Layer II infills depressions formed on this bedding surface. A sequence of mudflows (Layer I/a–f) rapidly covered the entire river bedding and its exposed banks. **d**, Mould of a freshwater gastropod (*Cerithidea*) from sandy Layer II. **e**, Detail of the locally developed, gradual boundary between sandy Layers II and muddy Layer I. Note the abundance of muddy rip clasts around the transition. At other places, the boundary is sharp. **f**, West baulk of E-32C. Large *Stegodon florensis* bones occur at the boundary between Layers II and I.

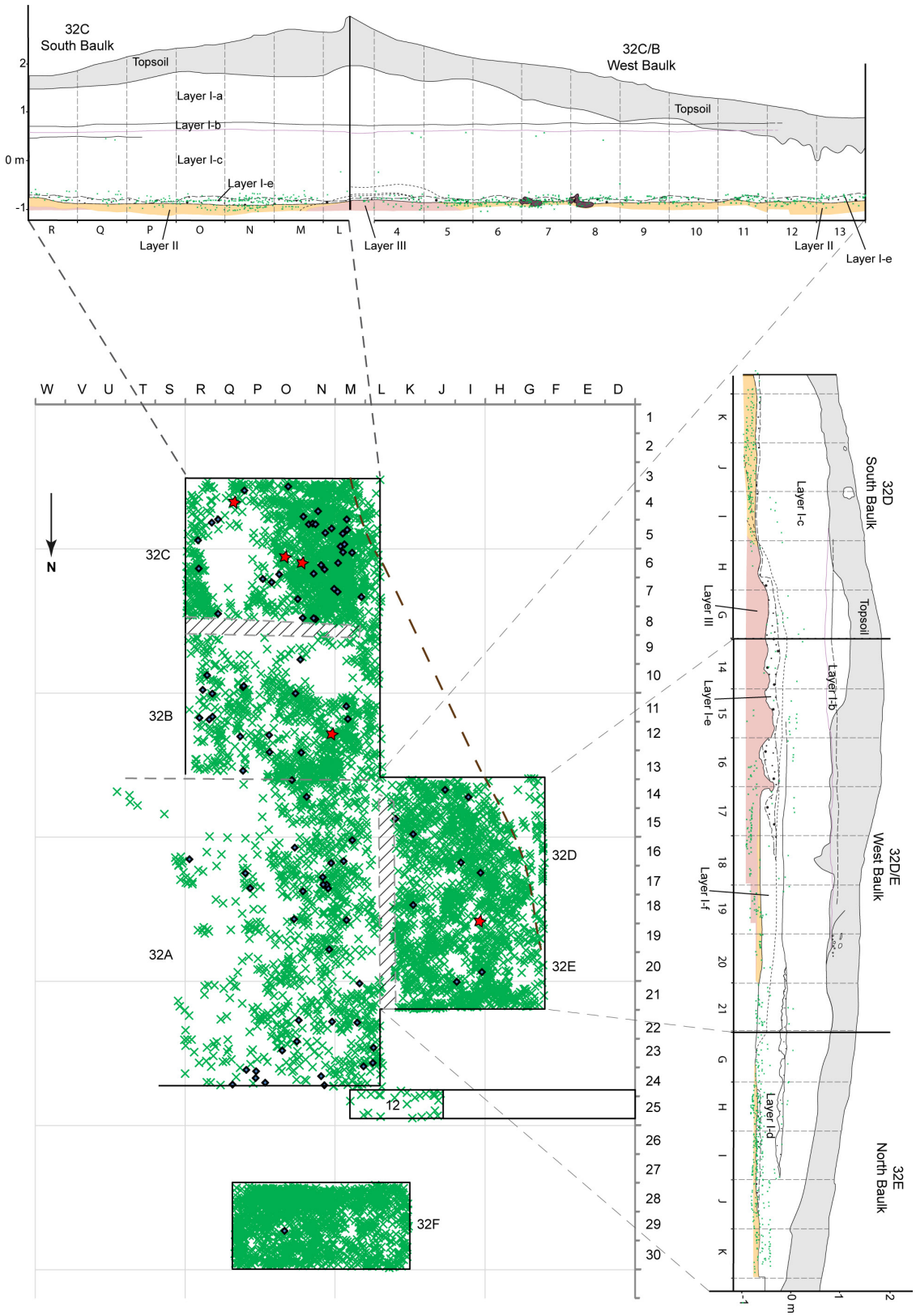

Extended Data Figure 2 | Plan and baulk profiles of Excavation 32A-F showing distribution of finds. The horizontal plan (lower left corner) shows the horizontal coordinates of individual fossil finds (green crosses) and stone artefacts (blue diamonds). The position of hominin fossils is indicated with red stars. In the trench baulk profiles (top and right) only the projected positions of fossil finds occurring within one meter of the baulks are plotted. All hominin fossils were recovered from the top of sandy Layer II. The basal part of the mudflow unit (Layers Ia–e) also contains fossils, stone artefacts, gastropods, and pebbles. The thick brown dotted line indicates the western margin of the ancient stream bed.

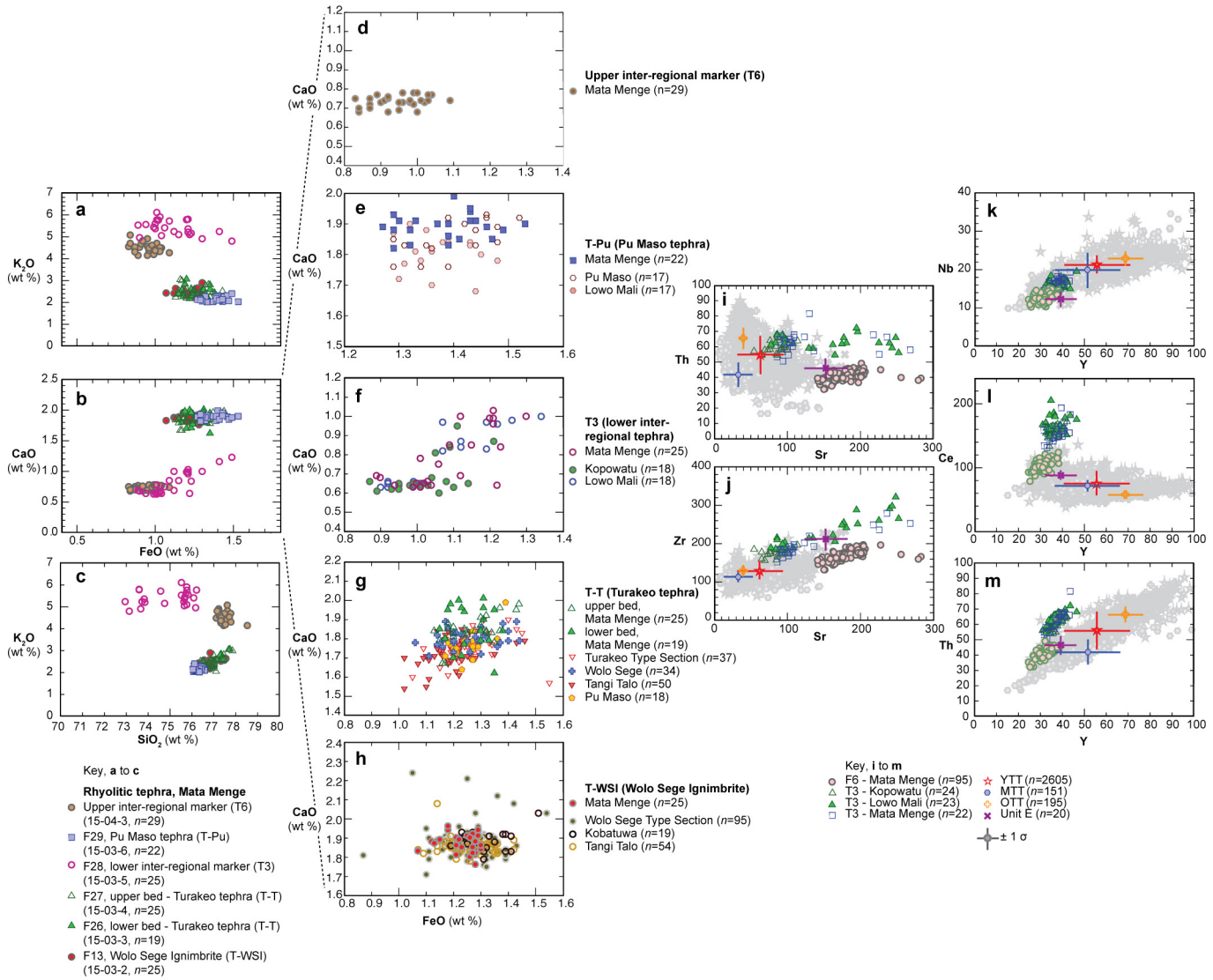

Extended Data Figure 3 | Glass shard geochemistry. a–c, Selected major element compositions (weight percent FeO vs K_2O, FeO vs CaO and SiO_2 vs K_2O) of glass shards from key rhyolitic pyroclastic density current (PDC) and airfall deposits at Mata Menge. **d–h**, Weight percent FeO versus CaO composition of glass shards from key rhyolitic pyroclastic density current (PDC) and airfall deposits at Mata Menge (in stratigraphic sequence from youngest to oldest) compared with correlatives from adjacent So'a Basin sites. While the major element glass compositions of T-WSI, T-T and T-Pu are all geochemically indistinguishable (they are most likely from the same eruptive source) the major element data for each of the tephra consistently occupies different overlapping fields. Moreover, while subtle geochemical differences exist between T-WSI, T-T, and T-Pu, these tephra can also be readily distinguished in the field by a combination of stratigraphic position and association, as well as by morphological expression. **i**, **j**, Selected trace element compositions Sr versus Th and Zr, and **k–m**, Y versus Nb, Ce and Th of glass shards from T3 correlatives at Mata Menge, Lowo Mali and Kopowatu as well as T6 (uppermost inter-regional marker) from Mata Menge. All trace element concentrations are in ppm unless otherwise stated. The data are plotted against equivalent elemental mean and standard deviation (represented as ± 1σ error bars) reference data from potential distal tephra correlatives (that is, Youngest Toba Tuff (YTT), Middle Toba Tuff (MTT), Oldest Toba Tuff (OTT) and Unit E from ODP-758) acquired on the same instrument using the same standards and under the same analytical conditions[41,42]. (YTT data source: Pearce, N. J. G., Westgate, J. A. & Gatti, E., Multiple magma batches recorded in tephra deposits from the Toba complex, Sumatra. V51F-3102, AGU Fall Meeting, San Francisco, 14-18 December 2015). Trace element data indicate that the upper (T6) and lower (T3) inter-regional marker beds occurring at Mata Menge cannot be geochemically related to any known Toba-sourced tephra. On this basis, the eruptive sources of T6 and T3 currently remain unknown. However, this absence of eruptive source does not diminish their importance within the overall So'a Basin stratigraphy.

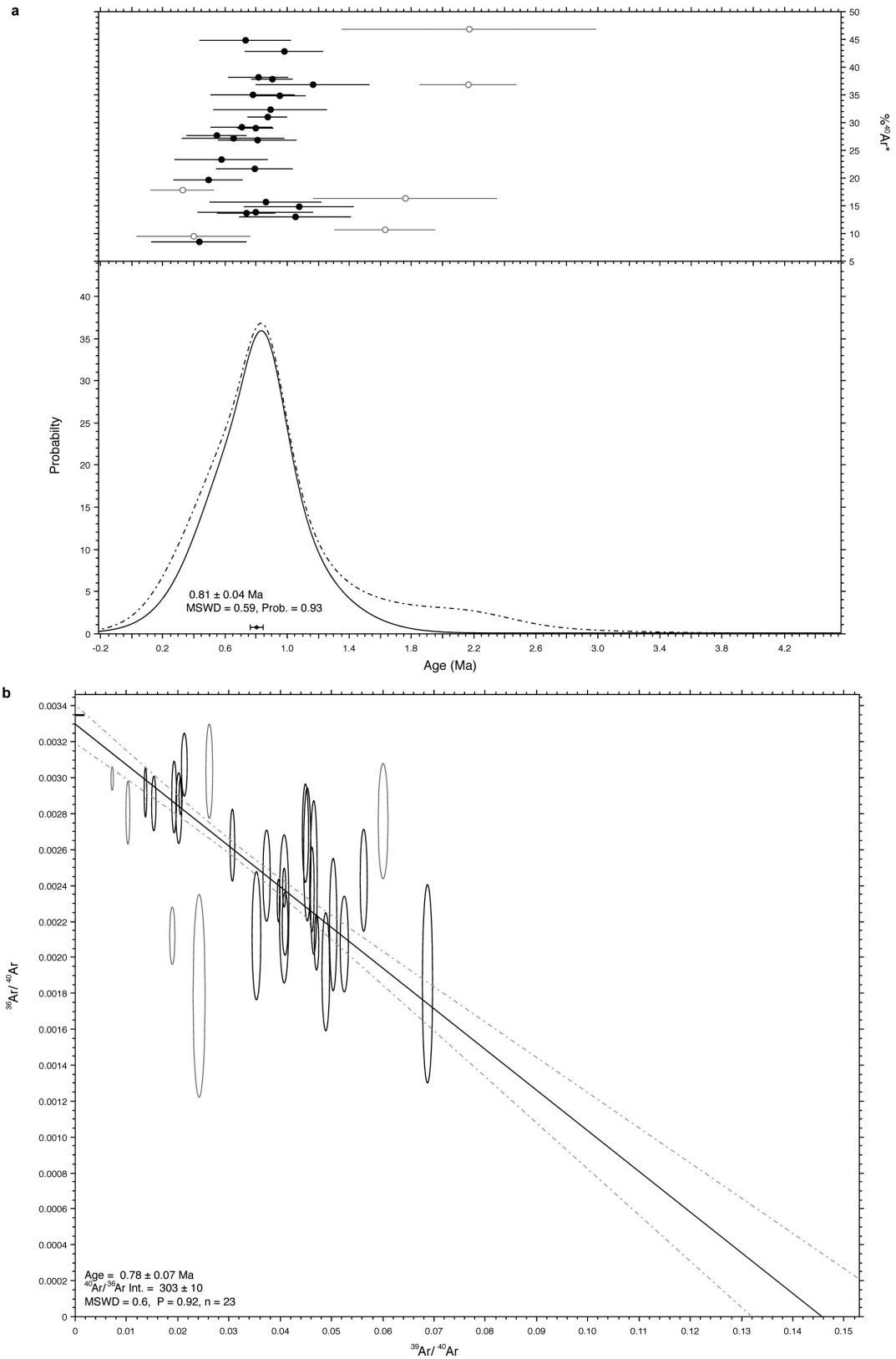

Extended Data Figure 4 | $^{40}Ar/^{39}Ar$ dating results. a, Age probability plot for single crystal laser fusion data for hornblende from the Pu Maso ignimbrite (sample FLO-15-15; Supplementary Information Table 5); the vertical scale is a relative probability measure of a given age occurring in the sample[57]. We applied an outlier-rejection scheme to the main population to discard ages with normalized median absolute deviations of >1.5 (ref. 58) and these are shown as open circles. $\%^{40}Ar^*$ refers to the proportion of radiogenic ^{40}Ar released for individual analyses. The weighted mean age of the filtered hornblende data for the Pu Maso ignimbrite is 0.81 ± 0.04 Ma (1σ; mean square of the weighted deviates (mswd) = 0.59, prob = 0.93; n = 23/29). **b**, An inverse isochron plot for these 23 analyses gives a statistically overlapping age of 0.78 ± 0.07 Ma (1σ; mswd = 0.6, prob. = 0.92). The $^{40}Ar/^{36}Ar$ intercept of 303 ± 10 is statistically indistinguishable from the atmospheric ratio of 298.6 ± 0.3 (ref. 59), thus supporting the more precise weighted mean age result.

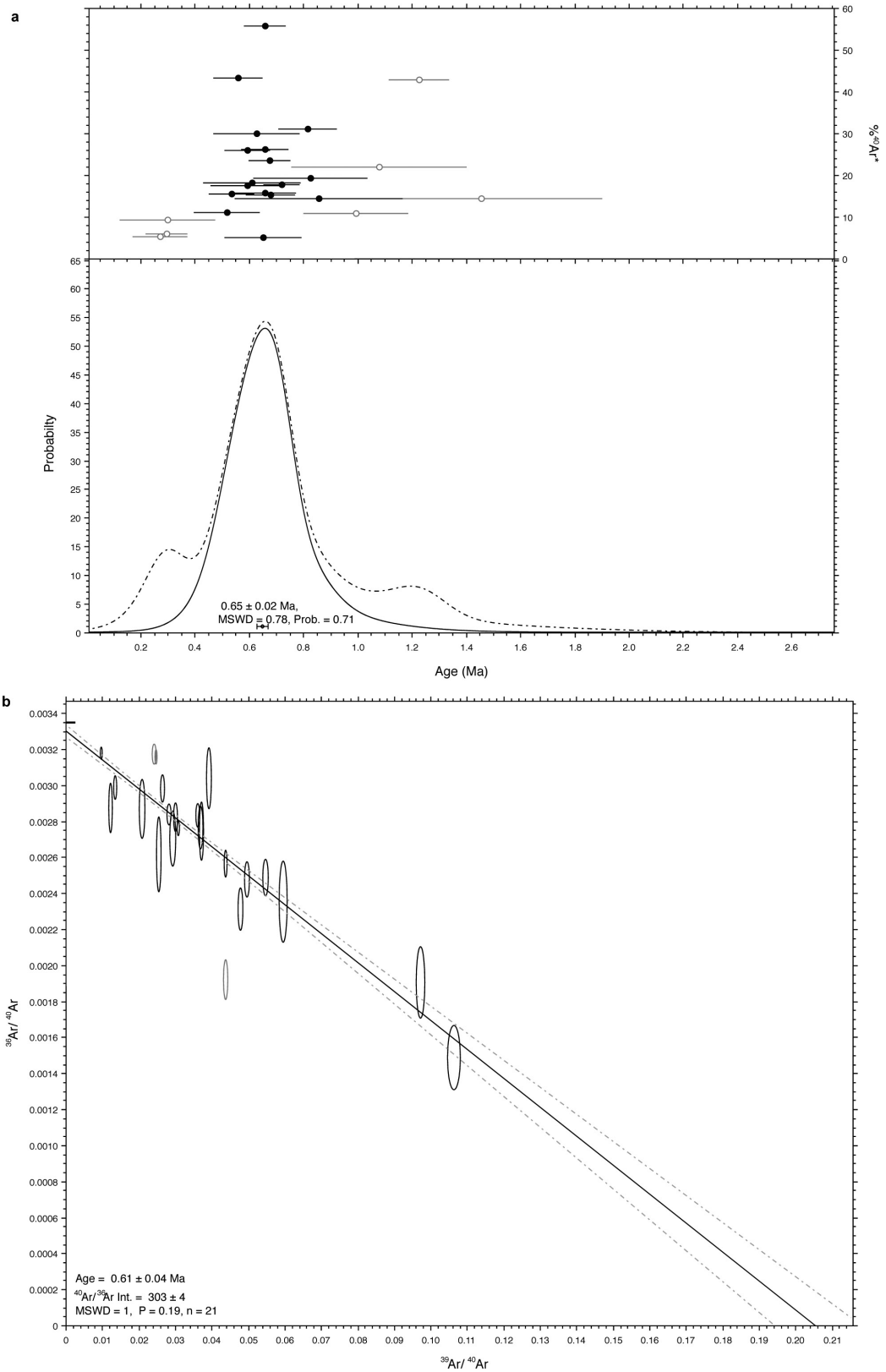

Extended Data Figure 5 | $^{40}Ar/^{39}Ar$ dating results. a, Age probability plot for single crystal laser fusion data for hornblende from the PGT-2 tephra (sample T XII 252-261; Supplementary Information Table 5). $^{40}Ar*$ ranges from <10% to nearly 60%. The weighted mean age of the filtered hornblende data for the PGT-2 tephra is 0.65 ± 0.02 Ma (1σ; mean square of the weighted deviates (mswd) = 0.78, prob = 0.71; $n = 17/24$). **b**, An inverse isochron plot gives a statistically overlapping, but less precise, age of 0.61 ± 0.04 Ma (1σ; mswd = 1, $P = 0.19$).

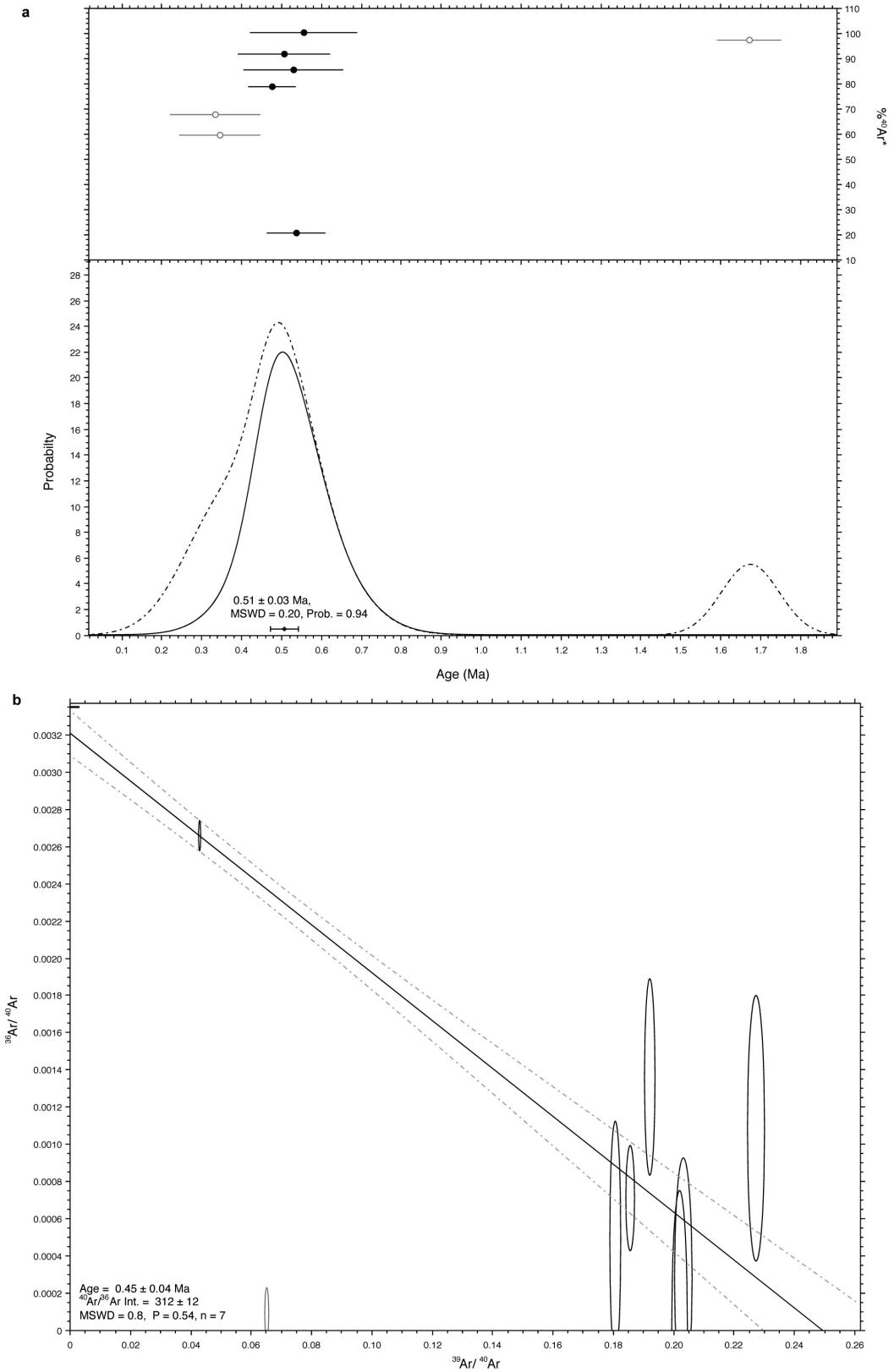

Extended Data Figure 6 | $^{40}Ar/^{39}Ar$ dating results. a, Age probability plot for single crystal laser fusion data for anorthoclase from the T6 upper inter-regional rhyolitic tephra (sample FLO15-09/2; Supplementary Information Table 5). $^{40}Ar^*$ ranges from 20% to nearly 100%. The weighted mean age of the filtered feldspar data for the T6 tephra is 0.51 ± 0.03 Ma (1σ; mswd = 0.20, prob = 0.94; $n = 5/8$). An inverse isochron plot (**b**) gives a statistically overlapping, but less precise, age of 0.45 ± 0.04 Ma (1σ; mswd = 0.8, $P = 0.54$).

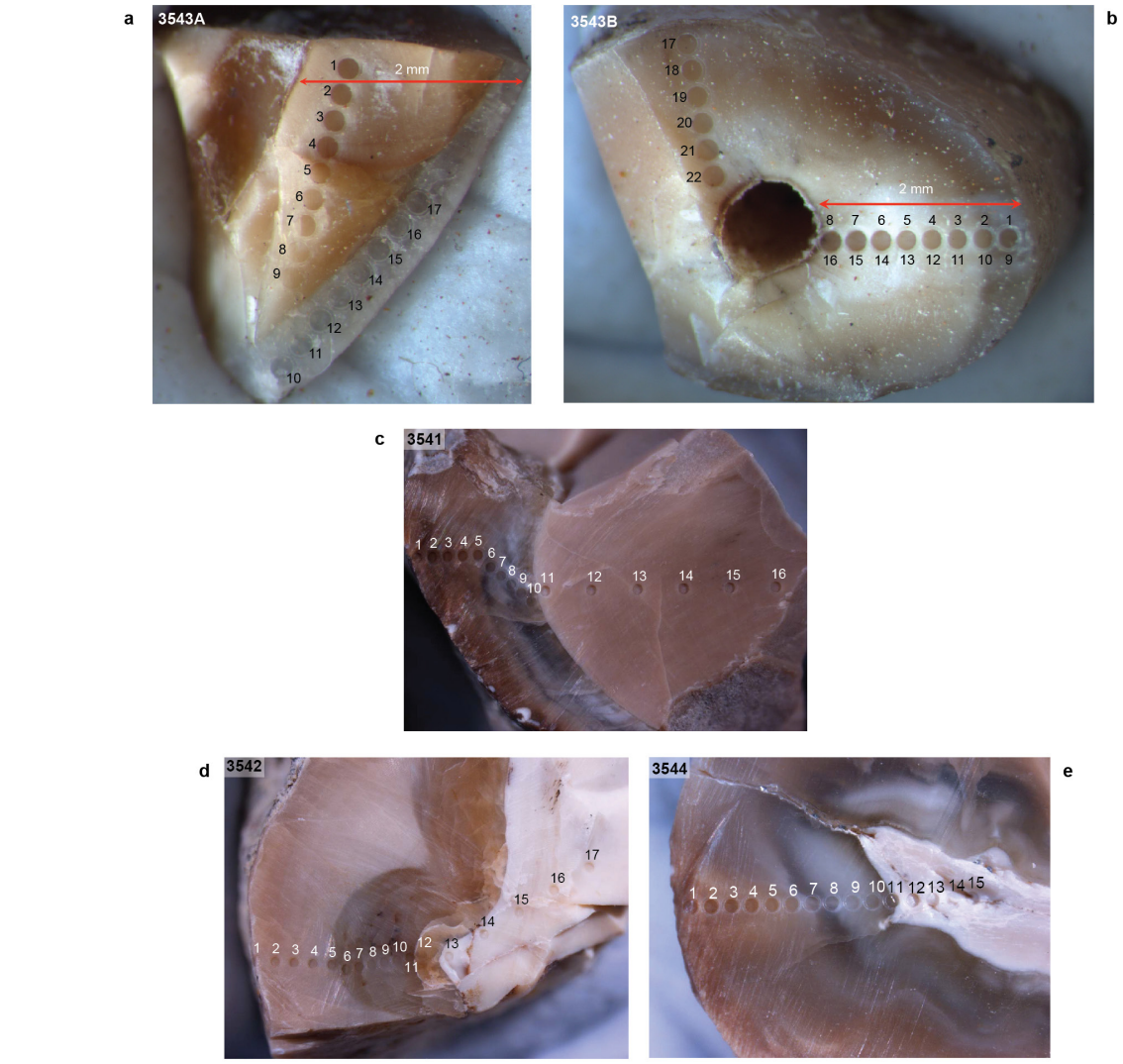

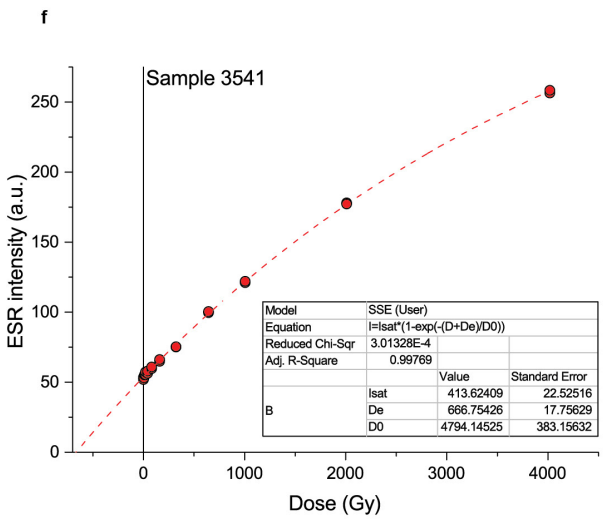

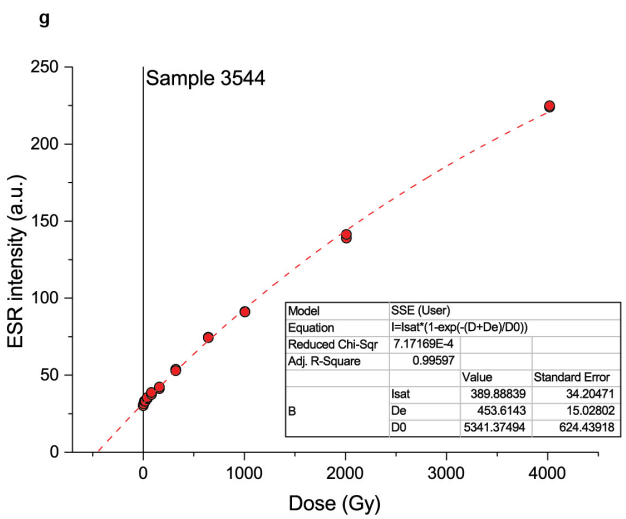

Extended Data Figure 7 | U-series and ESR samples and dating results. **a**, **b**, Hominin incisor (SOA-MM6) crown and root samples (number 3543A and number 3543B, respectively) from Layer II, Mata Menge. **c**–**e**, U-series laser tracks for *Stegodon* molar samples from Layer II. **f**, **g**, Dose response curves obtained for the two powder enamel samples from number 3541 and number 3544, respectively. Fitting was carried out with a SSE function through the pooled mean ESR intensities derived from each repeated measurement. Given the magnitude of the D_E values, the correct D_E value was obtained for $5 > D_{max}/D_E > 10$ (ref. 50).

a

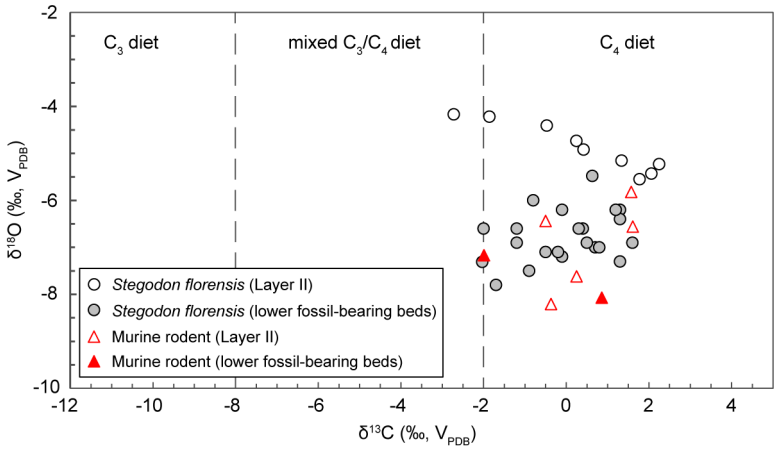

b

	Stegodon, lower levels	Murine rodent, lower levels	*Stegodon*, upper level (Layer II)	Murine rodent, upper level (Layer II)
Stegodon, lower levels (n=22)		0.251	0.281	0.3792
Murine rodent, lower levels (n=2)	0.251		0.2374	0.3329
Stegodon, upper level (Layer II; n=9)	0.281	0.2374		0.8542
Murine rodent, upper level (Layer II; n=5)	0.3792	0.3329	0.8542	

c

	Stegodon, lower levels	Murine rodent, lower levels	*Stegodon*, upper level (Layer II)	Murine rodent, upper level (Layer II)
Stegodon, lower levels (n=22)		1.00	**0.00287**	1
Murine rodent, lower levels (n=2)	1.00		0.6427	1
Stegodon, upper level (Layer II; n=9)	**0.00287**	0.6427		0.07229
Murine rodent, upper level (Layer II; n=5)	1	1	0.07229	

Extended Data Figure 8 | Carbon and oxygen isotope analysis of dental enamel. a, ^{13}C and ^{18}O values of *Stegodon florensis* and murine rodent tooth enamel. All but one of the $\delta^{13}C$ ratios correspond to a C_4 diet, indicating that the analysed *Stegodon* and murine rodents were predominantly grazers. The positive shift observed in ^{18}O of the younger *Stegodon* samples (from the hominin-bearing Layer II) is more difficult to interpret with the limited data available, but could mean a distinct source of drinking water (i.e., run-off versus lacustrine) and/or warmer conditions. **b**, Benferroni corrected *P* values for a pairwise Mann–Whitney statistical analysis to test for similarity of $\delta^{13}C$ between subsamples. **c**, Benferroni corrected *P* values for a pairwise Mann–Whitney statistical analysis to test for similarity of $\delta^{18}O$ between subsamples; *P* values showing significant differences in median values are in bold.

a

Trench	Layer	Assayed cobble	Flake	Multi-platform core	Bifacial core	Modified flake	Total
E-32A	I	1	9	-	-	-	10
	II	1	24	-	-	2	27
	III	-	5	-	-	-	5
	not determined	-	1	-	-	-	1
E-32B	I	-	34	2	1	2	39
	II	-	2	-	-	-	2
	III	-	2	-	-	-	2
	not determined	-	4	-	1	-	5
E-32C	I	-	7	-	-	-	7
	II	-	16	-	1	-	17
	III	-	1	-	-	-	1
	I, II interface	-	9	-	-	1	10
	not determined	-	3	-	-	-	3
E-32D	I	-	3	-	-	-	3
	II	-	1	-	-	-	1
	III	-	1	-	-	-	1
	II, III interface	-	2	-	1	-	3
	not determined	-	4	-	-	1	5
E-32E	I	-	2	-	-	-	2
	III	-	1	-	-	-	1
	not determined	-	2	-	-	-	2
E-32F	not determined	-	2	-	-	-	2
Total		2	135	2	4	6	149

b

Artefact type	Coarse- and medium-grained volcanics	Fine-grained volcanics and silicates	Total
Assayed cobble	2	–	2
Flake	90	45	135
Multiplatform core	1	1	2
Radial core	2	2	4
Retouched flake	2	4	6
Total	97	52	149

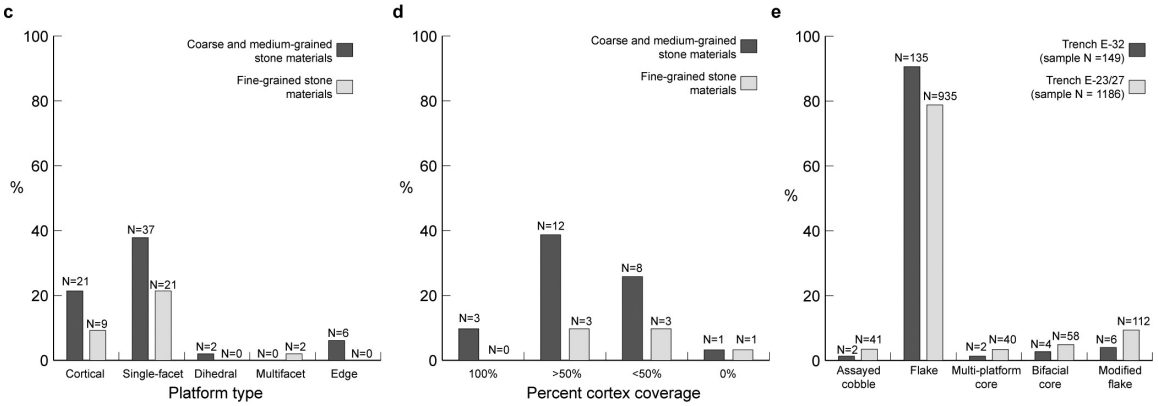

f

Artefact Type	Trench	Metrical summary		
		Largest linear dimension of complete artefacts (mm) (Mean ± SD, sample size)	Grams of complete artefacts (Mean ± SD, sample size)	Largest linear dimension of flake scars on cores and modified flakes (mm) (Mean ± SD, sample size)
Core	E-32	56.4 ± 31.9 (N=8)	189.9 ± 256.9 (N=8)	20.3 ± 12.8 (N=83)
	E-23/27	66.4 ± 27.4 (N=102)	294.1 ± 346 (N=102)	21.3 ± 13.5 (N=1116)
Flake	E-32	33.7 ± 13.5 (N=68)	15.6 ± 21.1 (N=70)	–
	E-23/27	41 ± 16.6 (N=450)	24.5 ± 28.7 (N=451)	–
Modified flake	E-32	34.9 ± 14.5 (N=6)	17 ± 24.8 (N=6)	–
	E-23/27	44.9 ± 16 (N=74)	39.1 ± 73.4 (N=74)	–

g

Trench	Coarse- and medium-grained volcanics	Fine-grained volcanics and silicates
	No, %	No, %
E-32	97 (65.1%)	52 (34.9%)
E-23/27	1025 (86.6%)	158 (13.4%)

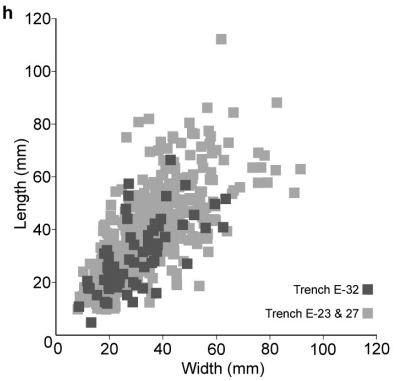

Extended Data Figure 9 | Analytical data for the Mata Menge stone technology. a, Artefact counts and provenance, trench E-32 (artefact definitions after ref. 60). **b**, raw materials used to manufacture the stone tool assemblage, trench E-32. **c**, Platform types on flakes and modified flakes, E-32. Cortical: the blow was struck onto the cortical surface of a cobble. Single-facet: the blow was struck on a scar produced by previous reduction. Dihedral: the blow was struck on the ridge between two scars produced by previous reduction. Multifacet: the blow was struck on the surface of multiple small scars produced by previous reduction. Edge: the blow was struck on the edge of the core and a platform surface is not retained on the flake. **d**, Cortex coverage on the dorsal surface of complete unmodified flakes, E-32. Percent cortex coverage refers to the proportion of the dorsal surface covered in cortex. **e**, Artefact counts, trenches E-32 and E-23/27 (artefact definitions after ref. 60). **f**, Sizes of artefacts and attributes, E-32 and E-23/27. **g**, Raw materials used to manufacture the stone tool assemblage, E-32 and E-23/27. **h**, Scatterplot of complete flake sizes, E-32 (total sample size $n = 68$ complete flakes) and E-23/27 ($n = 443$). With regards to raw materials, coarse- and medium-grained materials include andesite, basalt, rhyolite, and tuff. Fine-grained materials include silicified tuff, chalcedony, and opal.